Applied Catalysis B: Environmental 236 (2018) 253–264

Contents lists available at ScienceDirect

Applied Catalysis B: Environmental

journal homepage: www.elsevier.com/locate/apcatb

Au-doped Ni/GDC as an Improved Cathode Electrocatalyst for H_2O Electrolysis in SOECs

E. Ioannidou[a,b], Ch. Neofytidis[a,b], L. Sygellou[a], D.K. Niakolas[a,*]

[a] Foundation for Research and Technology, Institute of Chemical Engineering Sciences (FORTH/ICE-HT), Patras, GR-26504, Greece
[b] Department of Chemical Engineering, University of Patras, GR-56504, Greece

ARTICLE INFO

Keywords:
SOECs
Au-Ni/GDC electrode
H_2O electrolysis

ABSTRACT

The present work deals with the comparison between single electrolyte supported Solid Oxide Electrolysis Cells that comprise either a 3 wt.% Au-Ni/GDC or a Ni/GDC steam/hydrogen electrode. Specifically, their electrochemical performance was investigated for the H_2O electrolysis reaction by varying the pH_2O/pH_2 ratio (from 1 to 9), the operating temperature (800-900 °C) and the applied current. Physicochemical characterization was also performed both in the form of powders and as half cells with ex-situ and in-situ techniques, such as SEM, BET, XPS and TGA, including specific measurements in the presence of H_2O. Different structural and activity properties were observed for each cermet, where the cell comprising the 3Au-Ni/GDC electrode exhibited better electrochemical performance, especially at 850 °C and above, having lower polarization resistance. This improvement is ascribed to the formation of a surface Ni-Au solid solution, which causes weaker interaction of H_2O and of the resulting adsorbed O_{ads} species with the modified cermet. The outcome is an electrode with a lower degree of surface oxidation and increased "three phase boundaries" length, where the charge transfer and electrode processes are enhanced for the H_2O electrolysis reaction.

1. Introduction

H_2O electrolysis constitutes a promising method for the production of H_2 and O_2, with high purity and no pollution, by using electrical energy (Eq. (1)) [1]. One characteristic and recent application of this technology is electrolysis at high temperatures, by using Solid Oxide Electrolysis Cells (SOECs) [2–5]. Specifically, the electrical energy demand for the high temperature (600-1000 °C) H_2O electrolysis process, is much lower than the corresponding energy at low temperatures (< 100 °C), which yields significantly higher efficiency and performance in the former case [2–8]. In the case of SOECs, H_2O in the form of steam is fed to the cathode side, where it is reduced to hydrogen [reaction (2)]. Oxygen anions (O^{2-}) pass through the electrolyte to the anode, where they recombine to molecular oxygen, releasing two electrons (Reaction (3)) [6].

$$H_2O + \text{electrical energy} + \text{heat} \rightarrow H_2 + \frac{1}{2}O_2,\ \Delta H_f = 286\ \text{kJ/mol},\ \Delta G = 188\ \text{kJ/mol} \quad (1)$$

$$H_2O + 2e^- \rightarrow H_2 + O^{2-} \quad (2)$$

$$O^{2-} \rightarrow \frac{1}{2}O_2 + 2e^- \quad (3)$$

Although this technological application has considerable advantages, the development of SOECs is still at the lab-scale due to stability issues that prevent the widespread use and commercialization. One of the most important is the deactivation of the fuel electrodes (H_2O/H_2), which is usually ascribed to nickel re-oxidation, coarsening and agglomeration during H_2O electrolysis [2,9–11], or/and carbon deposition during H_2O/CO_2 co-electrolysis [10–15]. Another disadvantage is the degradation/delamination of the oxygen electrodes [9,16,17].

Recent research activities focus on the development and investigation of new/tolerant fuel and oxygen electrodes, optimization of operating conditions and adequate utilization of external heat sources [2,3,18–20]. The commonly used materials in SOECs are basically the same like those used for SOFCs [21] and up to now Ni-based/YSZ cells with different oxygen electrodes (e.g. LSM-YSZ, LSCF, LSM etc.) are the most investigated [2,3]. Despite the fact that Ni-based/YSZ cathode electrodes have demonstrated excellent initial performance for H_2O, CO_2 and co-electrolysis of H_2O plus CO_2, there are various reports that stress the poor durability either in the form of single cell measurements or in stacks [10,13,18,22–24]. In response to these failures, novel Ni-based SOEC cathode electrodes are continuously being processed for the H_2O and H_2O/CO_2 (co)-electrolysis processes [20,25,26]. Moreover,

* Corresponding author.
E-mail address: niakolas@iceht.forth.gr (D.K. Niakolas).

https://doi.org/10.1016/j.apcatb.2018.05.017
Received 27 November 2017; Received in revised form 30 April 2018; Accepted 7 May 2018
Available online 08 May 2018

incorporation of nanoparticles with high ionic conductivity and/or outstanding catalytic activity can lead to an effective enhancement of the performance, tolerance and stability of the state-of-the-art Ni-based electrodes.

Specifically, Lohsoontorn et al. [27] studied steam electrolysis on i) $CeO_2(Gd_2O_3)$ (GDC) - impregnated Ni/YSZ cathodes and on ii) 0.5 wt.% Rh-GDC impregnated Ni/YSZ and compared their performance with Ni/YSZ and Ni/GDC. One key finding from their investigation was that the GDC impregnation on Ni/YSZ electrodes could prove to be a simple and effective way to increase the long-term operation of SOECs [27]. Nishida et al. [28] developed a high performance hydrogen electrode, for reversible SOFCs/SOECs operation, based on Ni-Co coated samaria doped ceria (SDC) spherical particles. Specifically, the $Ni_{80}Co_{20}$/SDC composite electrode had the best performance for H_2O electrolysis and this was ascribed to the establishment of a conduction network for electrons and oxygen ions. Furthermore, the group of Bae and Lohsoontorn [29] investigated the electrochemical performance of Ni/YSZ, Ni/GDC and Ni-Ru/GDC as cathodes for H_2O electrolysis, CO_2 electrolysis and co-electrolysis processes. The major conclusion was that the Ni/GDC electrodes exhibited better performance under electrolysis conditions. However, according to the authors GDC has the drawback that increases the overpotential, with increasing the H_2O/H_2 ratio. Finally, the Ni-Ru/GDC cathode provided the highest performance for the co-electrolysis process, suggesting the latter as a possible improved Ni-based cathode [29].

Ni/GDC electrodes have been also reported from our research group as effective in preventing coke build-up with humidified CH_4 fuels, including the presence of H_2S impurities. In these studies and reviews [30–36] NiO/GDC was investigated either unmodified or modified with trace amounts of metals like Au and Mo and in regards to the doping level of gold, the amount of 3 wt.% was indicated as an appropriate loading. Apart from Solid Oxide Fuel Cells (SOFCs) applications, the use of the above materials in SOECs as H_2O/H_2 electrodes (cathodes) is also of high interest. The aim of this work is a continuation of our previous research, by studying and testing the commercial Ni/GDC (Marion Technologies) as well as the Au-modified Ni/GDC electrocatalyst in the SOEC H_2O electrolysis process. Complementary characterization was also performed both in the form of powders and as half cells with ex-situ and in-situ techniques, including specific redox stability measurements under various H_2O/H_2 feed conditions. According to the so far knowledge of the authors, the presented study deals for the first time with the experimental investigation and comparison of Au-modified Ni/GDC as SOEC cathode. Furthermore, the correlation of the presented findings with theoretical investigations is once again one of the first attempts in literature.

2. Experimental

2.1. Preparation of 3Au-NiO/GDC cermet, with nominal loading 3 wt.% of Au

The 3Au-NiO/GDC sample was prepared via the Deposition - Precipitation (D.P.) method. Commercial NiO/GDC powder (65 wt.% NiO - 35 wt.% GDC, Marion Technologies) was used as the support, which was immersed into triple distilled H_2O solution. The resulting suspension was mildly stirred and the temperature was adjusted to 70 °C. Appropriate volume of hydrogen tetrachloroaurate ($HAuCl_4$) (Sigma-Aldrich) was added in the suspension. During the deposition – precipitation of gold the pH value of the suspension was continuously adjusted in the region 7.0–7.1 with the addition of proper amount of aqueous NH_3 1M solution, which is the precipitant agent [30]. After filtering, the precipitate was repeatedly washed to eliminate the Cl^- anions and then it was dried at 110 °C for 24 h. The dried powders NiO/GDC (unmodified) and 3Au-NiO/GDC were calcined at 600 °C for 90 min and a portion of them at 1100 °C for 75 min. The former batch was used for the paste-preparation for the electrodes and the batch at 1100 °C was used for the physicochemical characterization of each sample.

2.2. Preparation of single Solid Oxide Electrolyte-Supported Cells

The single Solid Oxide Electrolysis Cells (SOECs) comprised circular shaped planar electrolyte (8YSZ)-supported membranes manufactured by Kerafol with a diameter of 25 mm and thickness of 150 μm. The fuel electrode was deposited by using the screen printing technique as reported in a previous study [33]. After the screen printing of the electrodes, the cells were sintered at 1150 °C for 2 h with a heating and cooling ramp rate of 2 °C/min. The applied temperature results in proper adhesion of both electrodes on the electrolyte, whereas it is quite similar to the calcination temperature (1100 °C) of the characterized powders. The loading of the examined cathodes was 10 mg/cm^2 with 1.8 cm^2 geometric surface area and a thickness of approximately 20 μm. The anode (O_2) side was a porous $La_{0.6}Sr_{0.4}Co_{0.8}Fe_{0.2}O_{3-\delta}$ (LSCoF) (provided by SOLIDpower). This electrode was also applied by means of screen printing and the final loading was 10 mg/cm^2. Furthermore, an adhesion layer (5 mg/cm^2) of GDC was used between the LSCoF electrode and YSZ electrolyte in order to overcome the thermal and chemical mismatch of the above materials (see Fig. S1 in supporting information).

2.3. Physicochemical Characterization

The samples either in the form of powders or as half cells were characterized with, SEM, BET, XPS and TGA redox stability measurements.

Measurements of Specific Surface Areas (SSAs) were obtained with the use of a Micromeritics Gemini V apparatus employing nitrogen physisorption at the temperature of liquid nitrogen (77 K).

The redox properties of the powders were investigated in a TA Q50 instrument with isothermal TGA measurements in the temperature range of 650–800 °C for the catalytic dissociation reaction of H_2O. Before each measurement, the samples were reduced in-situ with 80 vol. % H_2/Ar at 800 °C for 100 min. The isothermal TGA experiments were carried out under 15.5 vol. % H_2O/Ar with a total flow rate of 120 cm^3/min and the loading of the measured samples was approximately 50 mg. The addition of steam in the feed was achieved by passing Ar, as a carrier gas, through a saturator which was maintained at a constant temperature (65 °C).

Finally, the surface analysis studies were performed in a UHV chamber ($P < 10^{-9}$ mbar) which consists of a high pressure cell, where exposure of samples to several gas feeds may occur, a preparation and an analysis chamber. The analysis chamber is equipped with a SPECS LHS-10 hemispherical electron analyzer and a non-monochromatized dual-anode x-ray source for XPS. The XPS measurements were carried out at room temperature using AlKa radiation under conditions optimized for maximum signal (constant ΔE mode with pass energy of 97 eV giving a full width at half maximum (FWHM) of 1.7 eV for the $Ag3d_{5/2}$ peak). The analyzed area was an ellipsoid with dimensions 2.5 × 4.5 mm^2. The XPS core level spectra were analyzed using a fitting routine, which allows the decomposition of each spectrum into individual mixed Gaussian-Lorentzian components after a Shirley background subtraction.

Specifically, NiO/GDC and 3 wt.% Au-NiO/GDC, in the form of a half cells, were placed in the analysis chamber for XPS measurements. In each case the “pristine” sample was prepared via the screen printing method, as described above, and it was calcined at 1100 °C for 120 min in air. After the XPS measurements the sample was transferred to the high pressure chamber and it was heated in H_2 atmosphere at 615 °C for 12 hours. Sequential XPS measurements were recorded in the analysis chamber without exposing the reduced sample in air (1st reduction step). After this step, the half cell was ex-situ re-oxidized by heating at 1100 °C in air, for 90 min, and the reduction cycle in the high pressure

chamber of the XPS set-up was repeated (2^{nd} reduction step).

Wide Scans showed the presence of Ce, Ni, Au, C and O atoms, while the core level peaks that were recorded in detail were: Au4f, C1s, O1s and a combined window Ce3d-Ni2p. Errors in our quantitative data are found in the range of ~10% (peak areas), while the accuracy for BEs assignments is ~ 0.1 eV.

2.4. Electrocatalytic measurements

The electrocatalytic experiments were carried out in galvanostatic mode in the temperature range of 800-900 °C under H_2O electrolysis conditions, by applying different pH_2O/pH_2 ratios. Particularly, H_2O was introduced in the system in the form of steam. Prior its evaporation, liquid H_2O was circulated by means of a pressurized liquid H_2O vessel, which is connected to a mass flow controller. All lines and valves were heated at 160 °C to avoid H_2O condensation. Ni and Pt meshes were used as current collectors on the cathode and anode side, respectively. The cathode was pre-reduced before the electro-catalytic test under 100 vol.% H_2 (F_{total} = 150 cc min^{-1}) for 12 h. The evaluation of the electrochemical performance of Ni/GDC and 3Au-Ni/GDC cathodes, in single SOECs, was based on the recording of Current - Potential curves and simultaneous Electrochemical Impedance Spectra (EIS) characterization, which were carried out by using an AUTOLAB potentiostat/galvanonstat, model PGSTAT302 N with serial number: 84693. Specifically, the EIS were recorded in galvanostatic mode at various current densities and pH_2O/pH_2 ratios with an amplitude of 20 mA, in the frequency range between 100 kHz to 20 mHz. Other details regarding the experimental parameters are mentioned in the corresponding sections and/or figures.

3. Results and Discussion

3.1. Physicochemical characterization

BET measurements for the NiO/GDC, 3Au-NiO/GDC, NiO, GDC and for the corresponding reduced samples are shown in Table 1. The oxidized powders have similar specific surface area (SSA) depending on the sintering temperature. Specifically, at 600 °C all samples exhibit a SSA close to 5.2 m^2/g. By increasing the calcination temperature from 600 to 1100 °C, in air, the SSA decreased to 2.7-2.9 m^2/g for GDC, NiO/GDC and the 3Au-NiO/GDC samples. On the other hand, the SSA of NiO decreased significantly. The H_2-reduction of the samples at 850 °C induces further decrease to the SSA of Ni/GDC and 3Au-Ni/GDC by 41% and 26%, respectively. Finally, reduction of NiO dropped its SSA in such an extent that could not be accurately measured. It should be mentioned that the nominal loading of gold is 3 wt.% and the real loading was found [33], by means of ICP-OES, to be 2.3 wt.% of Au.

Fig. 1 shows SEM (top side) images of the Ni/GDC and 3Au-Ni/GDC electrodes in their reduced form. The images were collected in a HR – SEM (Zeiss SUPRA 35 V P). By comparing the (**1a**) and (**1b**) micrographs, one distinct observation is that the 3Au-Ni/GDC electrode has larger "void space", compared to Ni/GDC, which can be realized as higher porosity. The observed particles consist of Ni and GDC and their size, as indicated in the images, has been calculated in the range of 160 nm (std. error ± 4 nm) for Ni/GDC, while for 3Au-Ni/GDC in the range of 176 nm (std. error ± 4 nm).

Table 1
BET specific surface area S_{BET} of non-doped commercial NiO/GDC, NiO, GDC and modified Au-NiO/GDC powders. BET measurements took place on samples calcined at 600 °C, 1100 °C and after H_2-reduction at 850 °C. Error/accuracy of S_{BET} = ± 0.2 m^2 g^{-1}.

Sample powder	$S_{BET,\ 600}$ (m^2 g^{-1})	$S_{BET,\ 1100}$ (m^2 g^{-1})	S_{BET} (m^2 g^{-1}) (*reduced*)
NiO/GDC	5.3	2.9	1.7
3Au-NiO/GDC	5.4	2.7	2.0
GDC	5.5	2.9	2.2
NiO	4.5	0.7	< < 0.5

The surface chemical state of the samples, in the form of half cells, has been studied by means of XPS measurements. Fig. 2 shows the combined Ce3d-Ni2p window for the 3Au-NiO/GDC sample (see Fig. S2 in supporting information for Ni/GDC). Specifically, the Ce3d spectra can be resolved into three spin-orbit doublets $3d_{3/2}$; $3d_{5/2}$, called u and v, respectively. The u'', u''', v'' and v''' correspond to the satellite peaks of the u and v peaks, revealing the oxidation state of Ce in the case of CeO_2 (Ce^{4+}) and two main supplementary peaks u_0, u', v_0, v' in the case of Ce_2O_3 (Ce^{3+}) [37]. The binding energies of gold and nickel have been corrected for charging effects, by using the 917.1 eV, Ce u''', peak as internal reference. The Ni2p core level spectra consist of two spin-orbit doublets $Ni2p_{3/2}$ and $Ni2p_{1/2}$ with the characteristic shake-up satellites, which are most intense in the Ni^{2+} chemical state. In the case of Ce-Ni mixed oxides, the shake-up satellite peak of the $Ni2p_{1/2}$ level interferes with the $Ce3d_{5/2}$. Fig. 2 depicts that in the cases of the "pristine" and the re-oxidized sample the $Ni2p_{3/2}$ is at 855.5 eV and is assigned to Ni^{2+} chemical state (NiO or NiOOH), whereas in the reduced samples it is mainly in its metallic form [38].

The percentage of Ni^o and NiO in each step, after deconvolution of the $Ni2p_{3/2}$, is shown in Table 2, which summarizes the atomic surface concentrations of Au, Ce and Ni. The percentage of Ce^{4+} on the surface is also shown in Table 2 and it was calculated through the expression given by Yu and Li [37]. The latter formula uses the intensity ratio of u''' peak to the total Ce3d peak (u''' is the area fraction of the satellite at 917.1 eV and is attributed to Ce^{4+}).

The relative atomic concentration of Ce remains constant in the reduced Ni/GDC sample (see Fig. S2 in supporting information), while a marginal increase is observed in 3Au-Ni/GDC. Although the differences are not significant, they are reproducible and most probably can be related to the effect of Au on the structural properties of the formed Au-Ni solid solution [30] and its interfacial contact with GDC particles. In addition, Ce^{4+} is more reduced into Ce^{3+} in the case of 3Au-Ni/GDC, but in both samples the level of Ce^{4+} after the "re-oxidation" process is similar as that after the "1^{st} reduction". It should be noted that during the first reduction period Ni is partly reduced and 23-26% of Ni atoms remain in an oxidized form in both samples (Table 2). However, during the second reduction period the XP spectra show complete reduction of NiO to Ni. These observations may imply, restructuring and repositioning of the Ni and GDC particles during the successive re-oxidation and re-reduction of the samples. Specifically, partial incorporation of Ni atoms into GDC, as it has been reported in literature [39,40], could explain the incomplete reduction of NiO during the 1^{st} reduction period.

The Au 4f spectra are depicted in Fig. 3, where it is observed that the $Au4f_{5/2}$ level overlaps with the Ni3p shake up satellite (Fig. 3a). The small intensity of $Au4f_{5/2}$ corresponds to almost 3 times less than the nominal bulk loading of Au in the Ni/GDC sample. This is attributed to the relatively large size of the Au particles, which are dispersed on the NiO/GDC sample [30,34]. The large-sized particles are being formed during the high temperature (1100 °C) sintering of the 3Au-NiO/GDC electrode. Based on SEM images of the samples in their oxidized form, reported in previous studies [30,34], the particle size of Au is around 100 nm. Interestingly, upon reduction it was shown [30,34] that Au is no longer detected either by SEM, HR-TEM or by XRD analysis. However, in the herein presented XPS the Au4f doublet is more intense in the reduced electrode, than in the "pristine" oxidized sample, where it has specifically increased approximately 30 times. The amount of Au accumulated on the surface corresponds to ca. 8.9% of the surface Ni atoms. This is 9 times more than the bulk loading of Au (1 at.% with respect to Ni) in the Ni/GDC sample. It should also be noted that even though Au and Ni form a solid solution at the operating temperatures of the SOEC (800–900 °C) [41], Au atoms are still dispersed and accumulated on the Ni surface, as already published by the group of Prof. Nørskov [42,43]. Thus, according to the atomic ratios presented in

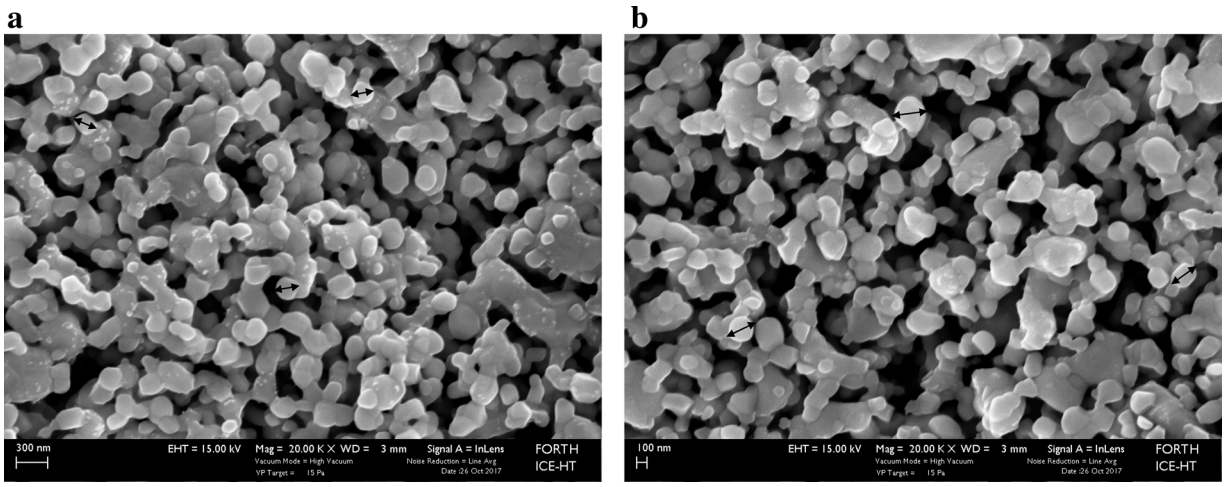

Fig. 1. a) SEM of the top (surface) side of the reduced Ni/GDC cathode layer. The black arrows depict indicative particles, for which the size was measured. The cell was calcined in air at 1150 °C for 2 h, with a heating/cooling rate of 2 °C/min. After calcination, it was reduced under 80 vol.% H_2/He (F_{total} = 70 cc/min) at 850 °C for 2 h, with a heating/cooling rate of 10 °C/min. b) SEM of the top (surface) side of the reduced 3 wt.% Au-Ni/GDC cathode layer. The black arrows depict indicative particles, for which the size was measured. The cell was calcined in air at 1150 °C for 2 h, with a heating/cooling rate of 2 °C/min. After calcination, it was reduced under 80 vol.% H_2/He (F_{total} = 70 cc/min) at 850 °C for 2 h, with a heating/cooling rate of 10 °C/min.

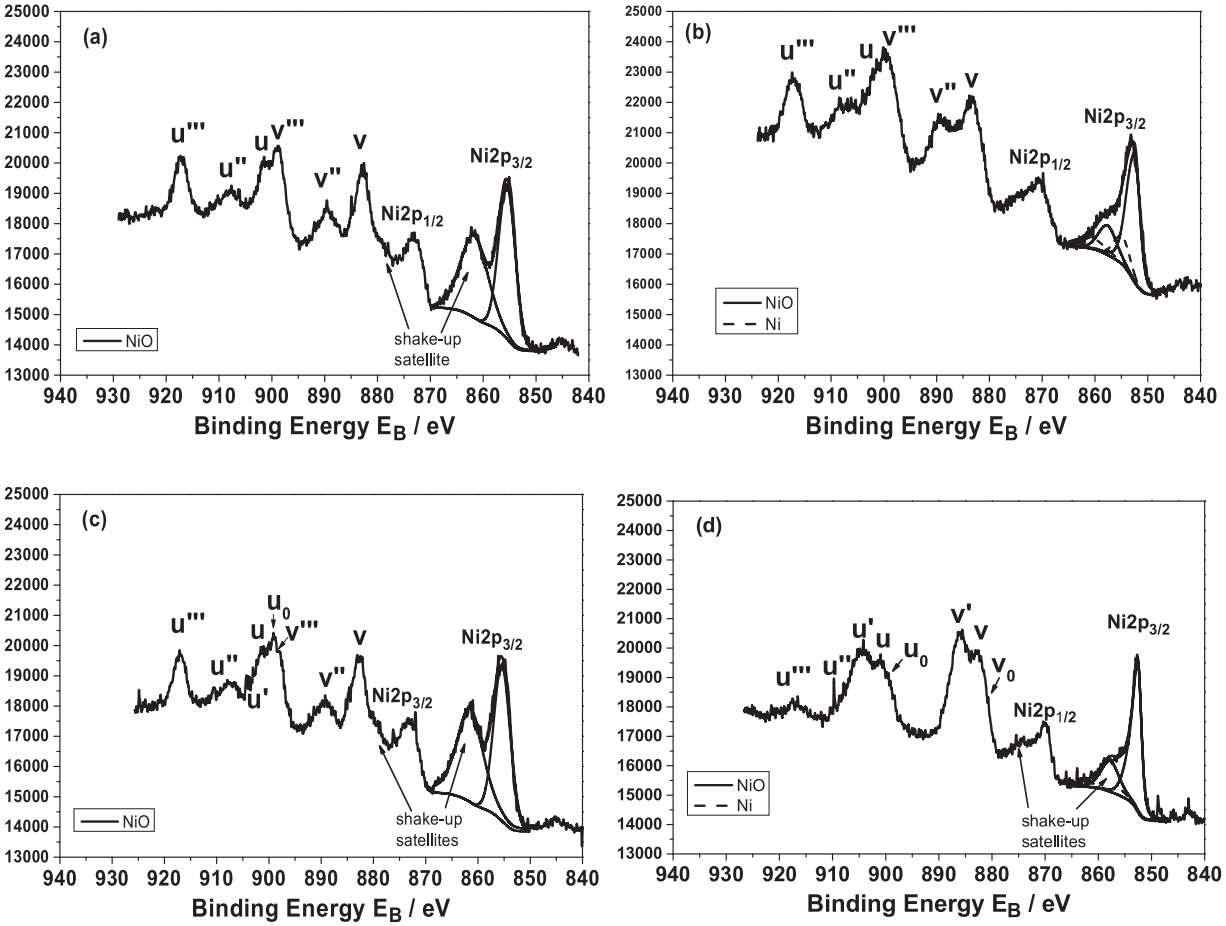

Fig. 2. A combined XPS Ni2p-Ce3d of 3 wt.% Au-NiO/GDC spectra of the (a) "pristine", (b) 1st in-situ XPS reduction (12 hours heating at 615 °C in H_2), (c) re-oxidation at 1100 °C in air and (d) 2nd in-situ XPS reduction.

Table 2 and the population of the surface nickel atoms, as calculated from the BET surface area of the samples in Table 1, it can be estimated that approximately 5% of the Au atoms must be atomically dispersed on the surface of the Ni particles. The selective interaction of Au and Ni has been proven in reference [30], showing a shift at lower 2θ values in the XRD peak of Ni metal particles, which was attributed to the formation of a solid solution between Ni and Au [30]. It is notable that Au is not detected at all in the XPS of the re-oxidized sample, most probably due to its coverage by the NiO, which is accumulated over the Ni/Au surface. Though Au is dispersed on the Ni surface, presumably at the

Table 2
Atomic surface concentrations of Au, Ce and Ni as measured through XPS for half cells comprising NiO/GDC and 3 wt.% Au-NiO/GDC as electrodes.

Sample	Relative atomic concentration		Binding Energy/eV (± 0.1)				
NiO/GDC	Ni	Ce	$Ni2p_{3/2}$	u'''/Ce3d	$\%Ce^{4+}$	%NiO	%Ni
"pristine"	1	0.64	855.5	0.14	100	100	0
1st reduction	1	0.63	852.9	0.13	92	23	77
re-oxidation	1	0.62	855.4	0.12	86	100	0
2nd reduction	1	0.65	852.7	0.095	68	0	100

Sample	Relative atomic concentration			Binding Energy/eV (± 0.1)					
3Au-NiO/GDC	Ni	Ce	Au	$Ni2p_{3/2}$	$Au4f_{7/2}$	u'''/Ce3d	$\%Ce^{4+}$	%NiO	%Ni
"Pristine"	1	0.59	0.003	855.4	83.9	0.14	100	100	0
1st reduction	1	0.75	0.089	853.0	83.85	0.093	66	26	74
re-oxidation	1	0.50	-	855.5	-	0.10	71	100	0
2nd reduction	1	0.69	0.088	852.6	83.85	0.025	18	5	95

atomic scale, the binding energy of Au4f in the reduced sample has similar value to the corresponding binding energy of the Au particles of the "pristine" oxidized sample. In fact, the formation of substitutional, random, metal Ni – Au solid solutions is not expected to induce any charge transfer from/to the Au atoms and this is because the two elements have similar size and electronegativity.

3.1.1. Interaction of the Water molecules with Ni/GDC and 3Au-Ni/GDC cermets

The redox properties of the powders have been also investigated with isothermal TGA measurements in the temperature range of 650-800 °C, under 15.5 vol.% H_2O/Ar feed conditions (Figs. 4 and 5). Fig. 4 depicts the isothermal at 800 °C TG analysis for Ni/GDC, Ni and GDC samples. It has to be mentioned that, up to now, the authors have not found any similar information in the literature for comparison reasons. The first observation is that low H_2 concentration in the feed (~

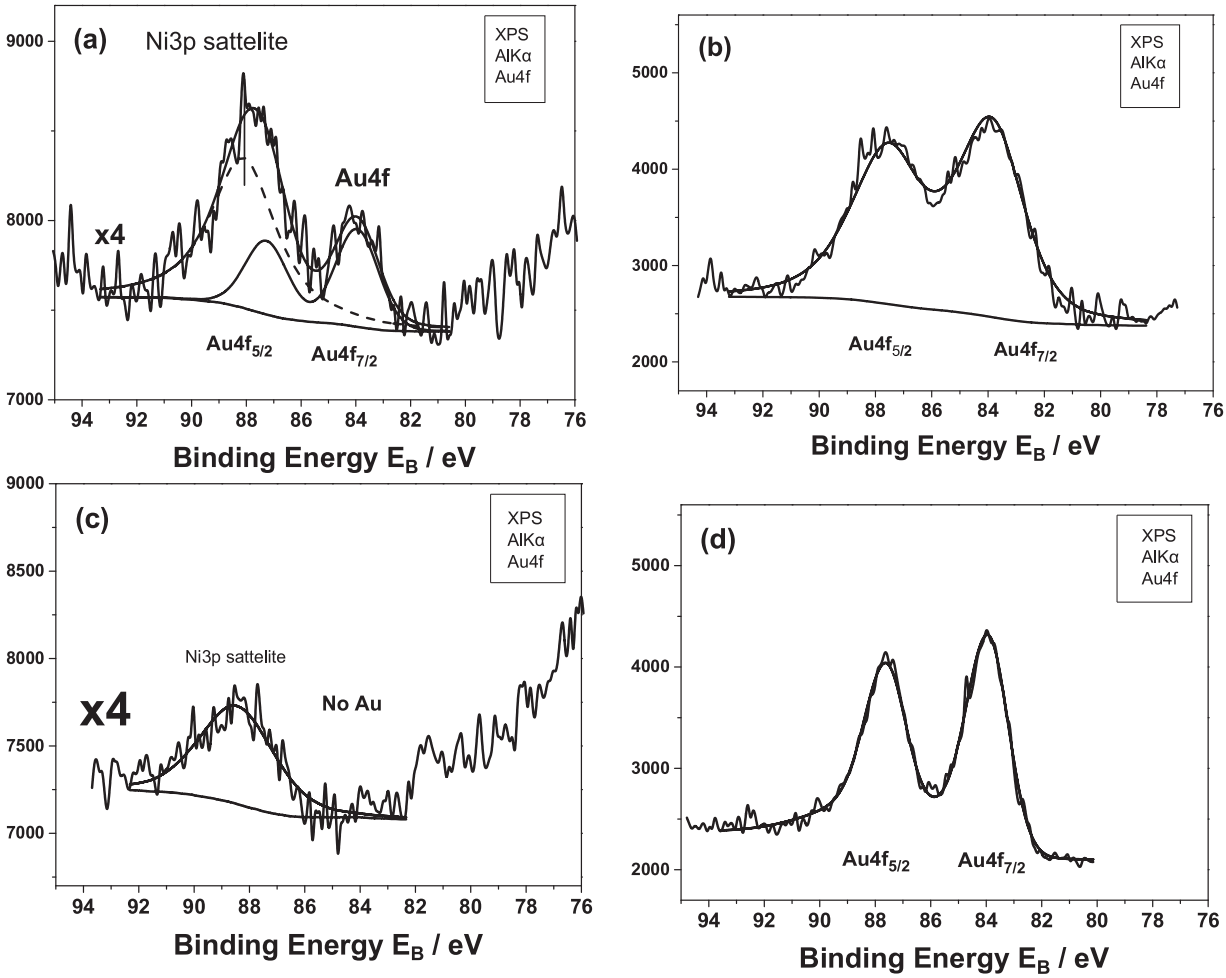

Fig. 3. Au4f XP spectra of 3 wt.% Au-NiO/GDC spectra of the: (a) "pristine", (b) 1st in-situ XPS reduction (12 hours heating at 615 °C), (c) re-oxidation at 1100 °C and (d) 2nd in-situ XPS reduction.

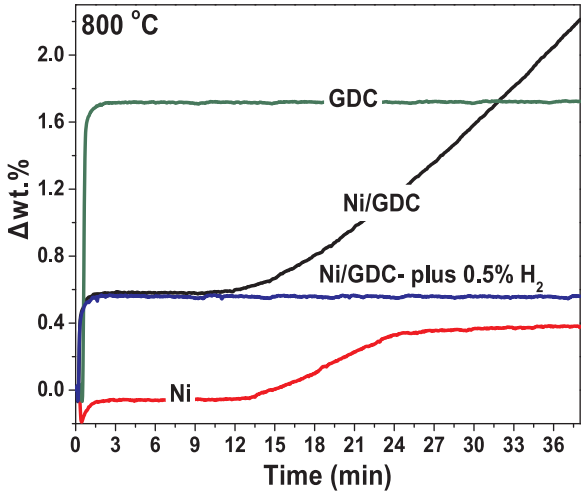

Fig. 4. Isothermal TG analysis at 800 °C under 15.5 vol.% H_2O/Ar feed conditions of the pre-reduced catalysts: Ni/GDC, Ni and GDC. The reaction conditions of 0.5 vol.% H_2 - 15.5. vol.% H_2O - Ar are also presented for Ni/GDC. F_{total} = 120 cc/min.

0.5 vol.%) protects Ni/GDC from bulk re-oxidation, owed to H_2O presence. This remark indicates that H_2-induced reduction is much stronger, compared to the H_2O-induced bulk oxidation. In the absence of hydrogen in the reaction mixture, H_2O acts as an oxidizing agent and in general it dissociates after adsorption, by reacting with the Ni atoms on the surface of the sample, for the production of H_2 and NiO [Reaction (4)].

$$H_2O + Ni \rightarrow H_2 + NiO \quad (4)$$

The TG profiles in Fig. 4 can be further divided in three sections with specific changes. Initially, a very fast and sharp increase in the weight can be attributed to the bulk re-oxidation of the partially reduced GDC and particularly of CeO_x (Ce^{3+} to Ce^{4+}). Similar changes correspond to the Ni/GDC sample. However, the lower initial increase in the Ni/GDC (where commercial NiO/GDC consists of 65 wt.% NiO and 35 wt.% GDC) is correlated to the lower wt.% content of GDC in the cermet. Taking into consideration that the reduction of GDC is realized through partial replacement of Ce^{4+} from Ce^{3+}, then the partial reduction of Ce^{4+} to Ce^{3+} corresponds to 36% of the former oxidative state. It is also noteworthy that the aforementioned weight changes in the TGA experiments are within the range of surface reduction of Ce^{4+} to Ce^{3+} (10-35%), as it is estimated by the XPS data in Table 2 (for the 1st reduction period).

Thereafter and specifically during the first 12 min of the reaction, Ni keeps its reduced state, since no changes in its weight (Δwt.%) are observed. This could be attributed to the prior formation of NiH in the bulk of Ni, during the reduction step of the samples. Thus, within the elapsed period of 12 min the formed NiH species dissociate and desorb H_2, which allows the electrode to stay in its reduced state. As it is explicitly shown in Fig. 5, the observed delay time period increases at lower temperatures, showing that this section is an activated process and corroborating the fact of the aforementioned NiH dissociation process.

In the third section of Fig. 4, which is after 12 minutes of operation, the weight of Ni/GDC and of Ni increases due to further re-oxidation of the sample, based on [Reaction (4)]. Despite the fact that this is a bulk oxidation, it is interesting to notice that the existing Ni amount in the samples is only partly oxidized. At the highest temperature the oxidation rate is approaching, asymptotically, a maximum oxidation degree, which corresponds to ca. 40% of the total Ni mass in the case of Ni/GDC and 1.5% in the case of Ni. Based on the surface area of Ni/GDC (1.7 m^2/gr, Table 1), one monolayer of adsorbed O_{ads} corresponds to 0.015 mg O_{ads}, or 0.074% increase in the weight of the sample. The amount of oxidized Ni corresponds to ca. 80 monolayers.

It is generally accepted that the H_2O-induced oxidation proceeds primarily through the dissociative adsorption of water molecules on the surface of the sample. Subsequently, there is diffusion of oxygen that oxidizes the surface of the sample and forms a NiO "crust", through which there is progressive diffusion of oxygen and oxidation of the bulk phase [44–46]. In this respect, the significantly lower oxidation degree of the Ni powder can be attributed to its quite low surface area and the limited diffusion rate of the O_{ads} species to the bulk of the Ni particles, especially after the formation of several layers of NiO. In the case of Ni/GDC, the presence of GDC results in increased SSA and promotes the reaction of Ni with water molecules through the interface of GDC with the Ni particles. This is concluded from the fact that the H_2O re-oxidation of GDC (Fig. 4) appears to be a much faster process than the corresponding re-oxidation of Ni. Moreover, the fast redox reactivity and oxygen exchange of CeO_2 and thus of GDC is reported as the main property for a strong metal/support interaction during the reduction and/or catalytic processes [47].

Fig. 5A and B show the isothermal TGA study of the unmodified Ni/GDC and Au-modified Ni/GDC powders, under 15.5 vol.% H_2O/Ar at 650, 700, 750 and 800 °C. For both samples there is always the "first-section" acute, but low weight increase, which is attributed to the complete bulk re-oxidation of Ce^{3+} to Ce^{4+}, described in Fig. 4. As mentioned above, by decreasing the temperature, the time duration of the first re-oxidation "delay" period increases (~ 25 min at 650 °C).

Another remark is that the interaction of Ni with Au affects the extent of re-oxidation. Specifically, the TG profiles showed that the 3Au-Ni/GDC sample (Fig. 5B) is slightly more tolerant than Ni/GDC against bulk re-oxidation by H_2O, for all studied temperatures. Decrease of the operating temperature from 800 to 650 °C inhibits the extent of bulk re-oxidation, as this is observed by the lower slopes. It must be also noted that the recorded rate is rather difficult to be influenced by oxygen diffusion limitations to the bulk of the Ni particles. This is because a similar experiment that was conducted under 7 vol.% O_2/Ar (see Fig. S3 in supporting information) resulted in oxidation rates more than one order of magnitude higher than those shown in Fig. 5. Thus, the slope of the linear part of the TG curves (Fig. 5A and B) represents the intrinsic dissociation rate of water and correspondingly the oxidation rate of the Ni atoms on the surface. In fact, one reason for the asymptotic approach of the Ni oxidation rate to zero can be attributed to the successive modification of the reactivity of the Ni surface atoms with the adsorbed H_2O. The latter modification is caused by the subsurface accumulation of the O_{ads} species that may affect the electronic and catalytic properties of the Ni atoms.

Fig. 5C compares the Arrhenius plots of the oxidation rates for Ni/GDC and 3Au-Ni/GDC, which have been calculated from the slopes of the linear part of the TG curves (Fig. 5A and B). It is observed that the rates of 3Au-Ni/GDC are lower than those of Ni/GDC. This is corroborated by the higher apparent activation energy ($E_{a,ap}$), defined from the Arrhenius plots. Specifically, the $E_{a,ap}$ in the case of Ni/GDC is 41 kJ/mol and in the case of 3Au-Ni/GDC increases to 56 kJ/mol. These values are well compared with those reported by Ghosh et al. [48], who applied DFT calculations for the catalytic dissociation of H_2O [Reaction (5)] on a Ni (111) surface and found the activation energy equal to 69 kJ/mol. In other DFT studies Gan et al. [49] reported similar activation barrier for Ni (111), equal to 86 kJ/mol, while Gu and Nikolla [50] computed higher activation energies for Ni (111) and Ni (211) surfaces, equal to 244 kJ/mol and 229 kJ/mol, respectively. The difference of the latter values has not been clarified yet, either by the authors of the published DFT studies or by us.

$$H_2O + Ni \leftrightarrow H_{ads} + OH_{ads} \quad (5)$$

Taking into account that the adsorption of water on Ni is facilitated through the oxygen bonding with Ni atoms, according to the "d-band center" theory and the reported examples from the group of Nørskov et al. [51,52], the surface solid solution between Ni and Au, causes a

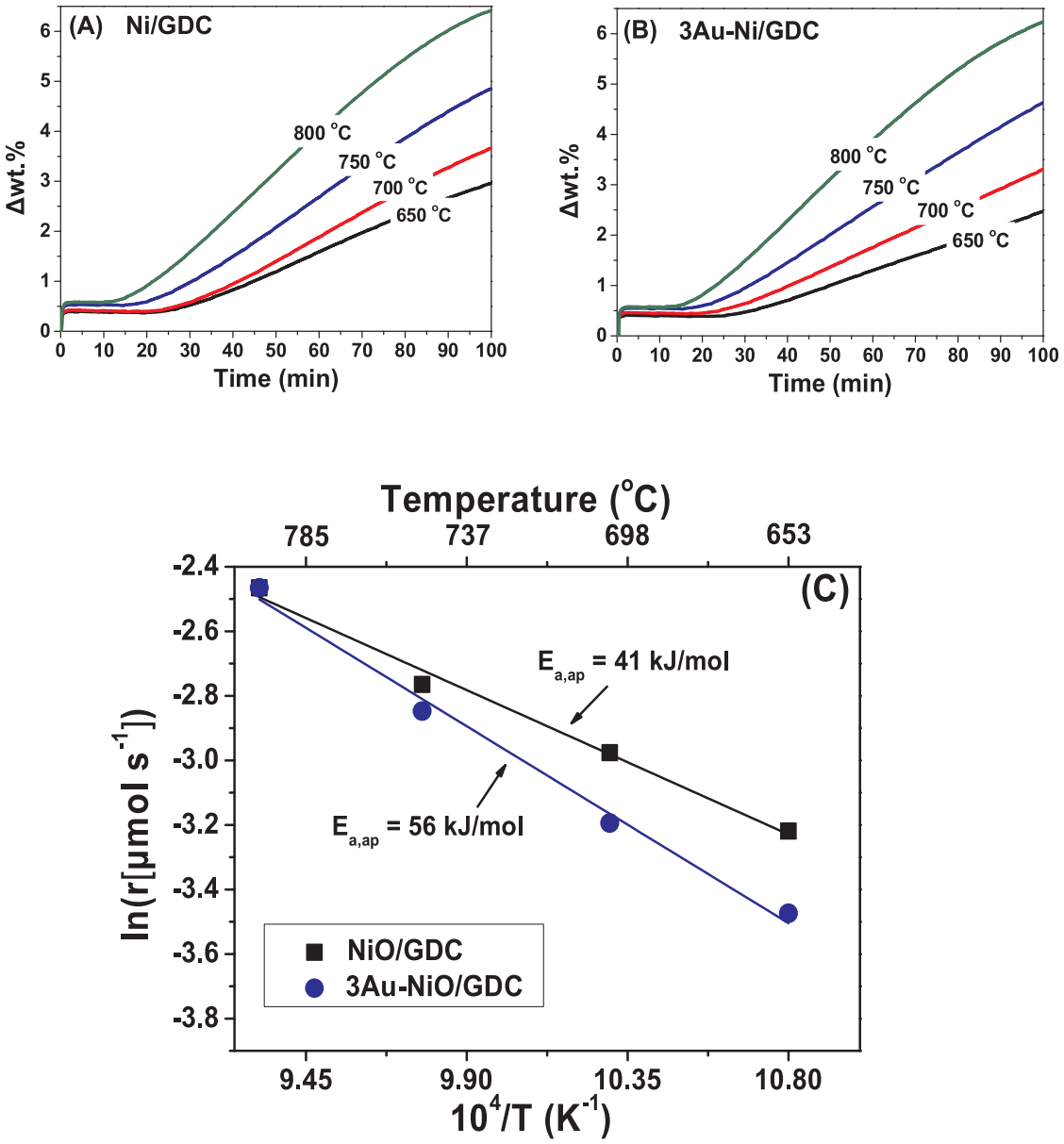

Fig. 5. Isothermal TG analysis of the pre-reduced (A) Ni/GDC, (B) 3 wt.% Au-Ni/GDC samples at various temperatures in the range of 650-800 °C and (**C**) Arrhenius plots for (■) Ni/GDC and (●) 3 wt.% Au-Ni/GDC. ***Feed Conditions***: 15.5 vol.% H_2O/Ar, F_{total} = 120 cc/min.

decrease of the metal`s d-band center to lower energies, below the Fermi level, thus resulting in the weakening of the bond of water with the modified Ni atoms. Respectively, based on the same considerations, the adsorbed oxygen from the dissociation of water, is also more weakly bonded on the Ni-Au surface. Moreover, the Arrhenius plots in Fig. 5C indicate the existence of an iso-kinetic point at 800 °C. This remark suggests that at temperatures lower than 800 °C the most active sample for the dissociation of H_2O is the one with the lower $E_{a,ap,}$ which is Ni/GDC. On the other hand, at higher temperatures (> 800 °C) the most active should be 3Au-Ni/GDC with the higher $E_{a,ap}$ and presumably with the lower binding energy for both H_2O and O_{ads}. Finally, the stronger binding of O_{ads} species that is suggested on Ni/GDC, can induce a poisoning effect on the Ni surface, leading to faster re-oxidation and finally deactivation of the sample, as already reported by Gu and Nikolla [50].

3.2. Electrochemical performance

The electrocatalytic measurements for the H_2O electrolysis reaction were performed by using YSZ electrolyte supported cells (ESCs), with a two electrode configuration (Fig. S1 in supporting information). In all cases the cathode feed was diluted in 30 vol.% He and the anode feed was pure (100 vol.%) O_2. Simultaneous EIS measurements were performed in an attempt to record and investigate the electrochemical effect of the H_2O electrolysis reaction conditions and of the occurring processes on the ohmic (R_{ohm}) and polarization resistance (R_{pol}) of the modified cathode electrodes. R_{ohm} is the sum of ohmic losses, including the contribution from the: (i) ionic resistance due to the O^{2-} transport through the YSZ electrolyte, (ii) electron resistance of the electrodes and specifically the part that can be electrochemically inactive and (iii) contact resistances of the connecting wires. R_{pol} is mainly related to the occurring electrode processes [53] and combines both activation and concentration polarizations. Specifically, the latter type is attributed to diffusion processes (i.e. diffusion of steam through the pores of the electrode to the triple phase boundary (t.p.b.) and diffusion of H_2 out of the t.p.b.) and to the conversion of steam at the cathode [54]. In EIS analysis the R_{ohm} value is obtained from the high frequency intersect on the real (Z') axis of the Nyquist plot and the total resistance of the cell

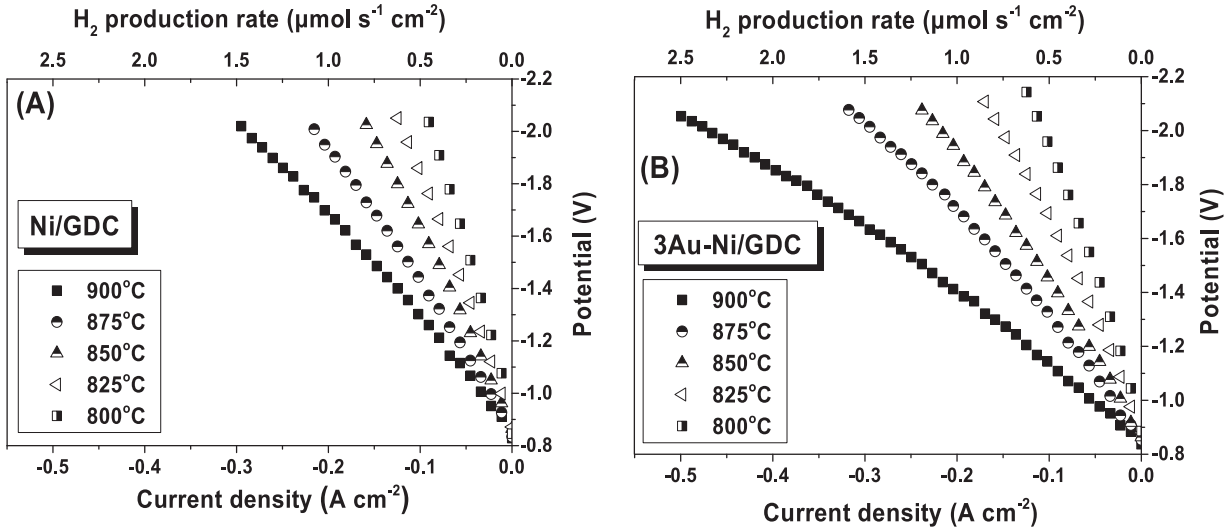

Fig. 6. I-V curves in the temperature range between 800– 900 °C for ESCs comprising (**A**) Ni/GDC and (B) 3 wt.% Au-Ni/GDC as cathode electrodes. The measurements took place under H_2O electrolysis conditions and the reaction mixture contained 63 vol.% H_2O, 7 vol.% H_2 and 30 vol.% He with F_{total} = 150 cc/min (pH_2O/pH_2 = 9).

(R_t) is obtained from the low frequency intersect on the real axis. R_t is the sum of ohmic and polarization resistances ($R_t = R_{ohm} + R_{pol}$) and by using this equation, R_{pol} is derived.

Fig. 6 depicts the comparison of performance between cells comprising Ni/GDC (**6A**) and 3 wt.% Au-Ni/GDC (**6B**) as cathodes. The presented results deal with the H_2O electrolysis process under the reaction mixture of 7% H_2-63% H_2O-30% He. It is observed that the Au-modified electrode exhibited significantly better electrochemical performance, than the cell with Ni/GDC, mainly at temperatures above 850 °C. Specifically, at 900 °C the cell with the 3 wt.% Au-Ni/GDC cathode showed lower overpotential losses with approximately double rates for the H_2O electrolysis reaction at the same potential. On the other hand, Bae and Lohsoontorn [29] reported that the modified Ru-Ni/GDC cathode showed worse performance than that of Ni/GDC, under H_2O electrolysis measurements. The improved electrocatalytic activity of the Au-modified cell, remained also under the various applied pH_2O/pH_2 ratios (see Fig. S4 in supporting information). The presented I-V curves in Fig. S4 have been derived after IR_{ohm} correction, in order to subtract any contribution from the ohmic resistances. It is also observed that by increasing the partial pressure of H_2O there is gradual improvement in the performance of both cells, due to the increase in the concentration of the fuel. The latter causes as well the decrease in the Open Circuit Potential (O.C.P.) values, according to the Nernst Eq. [(6)].

$$E_{O.C.P.} = E^0 - \frac{RT}{2F}\ln\left(\frac{P_{H_2O}}{P_{H_2}P_{O_2}^{1/2}}\right) \quad (6)$$

where: $E_{O.C.P.}$ and E° are the open circuit potential and standard potential, respectively, at a given temperature T.

The effect of the applied pH_2O/pH_2 ratios (at T = 900 °C) on the R_{ohm} and R_{pol} values of the examined cells is presented in Fig. 7. The comparison takes into account two requirements. The first is that the impedance spectra on each sample were recorded under similar values of applied current. The second is that the comparison is focused on EIS that lie within the same I-V region. It is observed that in both cases the R_{ohm} and R_{pol} values are relatively high. Specifically, for the ohmic resistance there is a great variety of values being reported in literature, where for similar type of YSZ-supported cells at 900 °C they are close to 0.9 Ohm cm^2 [55] and lower for State of the Art (SoA) systems [56]. The increased values in our case are mainly ascribed to the fact that the examined cells and the experimental setup are not SoA.

In particular, the combination of various factors such as: (i) the relatively thick (150 μm) YSZ electrolyte, (ii) the fact that the cathode electrode comprised only the studied functional layer, without other layers (e.g. adhesion and/or current collection layer), (iii) the low calcination temperature of the cathode electrode (1150 °C) [57] and (iv) the additional contact resistances from the experimental setup, resulted in increased R_{ohm} and R_{pol}. Furthermore, it has been reported [58] that the O_2 electrode configuration, comprising GDC/LSCoF, contributes as well to the observed high R_{ohm} values. Thus, considering that the examined cells had a two-electrode configuration, there was an effort to minimize the effects from the O_2 electrode. The latter was achieved by (i) trying to optimize the performance of the anode, using close to 10 mg/cm^2 of LSCoF as an optimum loading and (ii) by keeping constant reaction conditions on the O_2 side.

Another interesting remark is that the Au-modified cell exhibited lower R_{ohm} and R_{pol} values, which has been repeatedly observed at several experiments. This difference can be attributed, at this point, to improved structural properties of the Au-Ni/GDC electrode. Indicatively, the enhanced reducibility of this electrode with the increased amount of surface Ce^{3+}, as suggested by the XPS measurements, in combination with the re-oxidation resistivity provided by gold, may result in (i) higher electronic/ionic conductivity and (ii) better electrode/electrolyte interface.

By increasing the partial pressure of H_2O, at similar current densities, both cells exhibited (Fig. 7 and 8) an increase of their ohmic and polarization resistances. The former case is not related to an activated (i.e. electrochemical) process, but to the increase of electronic, ohmic resistance. This is shown in Fig. S5 (supporting information), which depicts the effect of temperature on the R_{ohm} difference (ΔR_{ohm}), between the highest (pH_2O/pH_2 = 9) and the lowest (pH_2O/pH_2 = 1) ratio, at similar current densities. It is observed that the increase of the ohmic resistance, in both cells, was constant and this is most probably attributed to the gradual surface oxidation of the Ni mesh (current collector), which increased the contact resistance of the electrode with the current collector. In general, this trend is one of the degradation reasons for SOECs, especially in long-term stability measurements [9,20,24,53,59]. In particular, a recent (post-mortem) study by Frey at al. [9] reports that the observed increase of the ohmic resistance, in the examined SOEC stack, is attributed to the gradual re-oxidation of Ni, especially at the inlet of the fuel, which causes gradual transportation of Ni, in the form of nickel hydroxides, and finally results in nickel depletion from that side of the cathode. Moreover, the increase of the ohmic resistance is frequently observed in short term measurements in

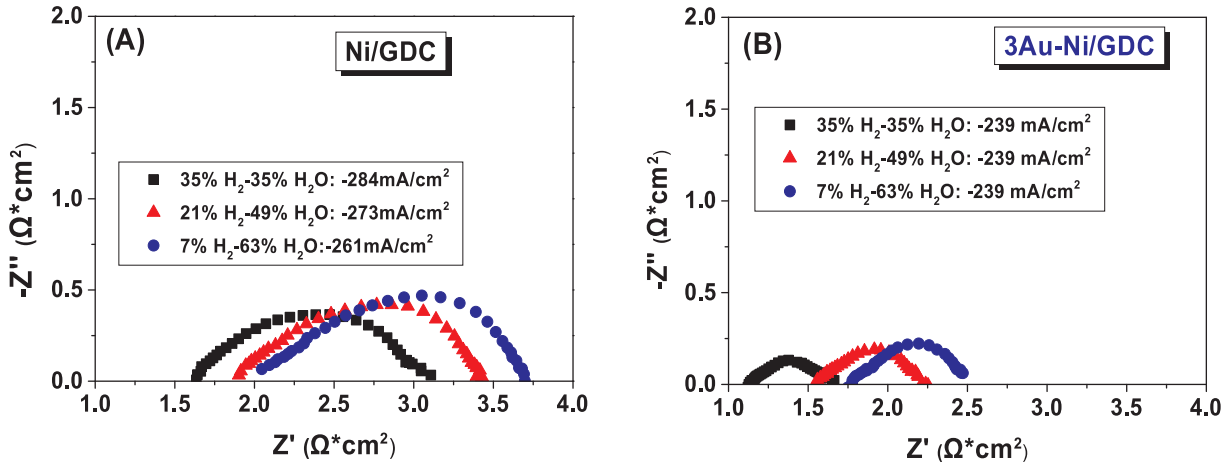

Fig. 7. EIS measurements (Nyquist plots) on electrolyte-supported cells comprising (**A**) Ni/GDC and (**B**) 3 wt.% Au-Ni/GDC as cathode electrodes for the H_2O electrolysis reaction. The spectra were recorded on galvanostatic mode at T = 900 °C and different pH_2O/pH_2 ratios: (■) 35/35 = 1, (▲) 49/21 = 2.3 and (●) 63/7 = 9. In all cases the reaction mixture was diluted in 30 vol.% He with F_{total} = 150 cc/min. The applied current is depicted in the figure.

lab-scale cells and experimental setups, like those in the presented study. In these cases one common approach is to deduct the pure ohmic contribution from the Nyquist plots [60]. Therefore, regardless on the type of measurement, the gradual increase of R_{ohm} can be ascribed to various reasons and one approach for interpretation is the one shown in Fig. S5.

In respect to the R_{pol}, Figs. 7 and 8 show that by increasing the applied pH_2O/pH_2 ratio, there was increase in the polarization resistance of both cells. However, in the case of the cell with 3Au-Ni/GDC the R_{pol} increment (ΔR_{pol} in Fig. 8) is less and overall the absolute R_{pol} values (Fig. 7B) are quite lower, compared to Ni/GDC (Fig. 7A). Thus, for pH_2O/pH_2 = 9 and for all the examined ratios (not shown here) the Au-modified electrode exhibited higher polarization conductance, as shown in Fig. 9.

Regarding Ni-based electrodes, the oxidation, coarsening and volatilization of nickel have been reported [9,61–63] as primary causes for the cathode deactivation. This can be realized through the formation of strongly adsorbed oxygen species and/or the subsequent formation of surface nickel hydroxide layers [9,64,65]. Oxidation of Ni reduces the electronic conductivity of the electrode, but it also induces nickel coarsening and volumetric expansion [44], which are related to the decrease of the (t.p.b.) length and the concomitant increase of the cell

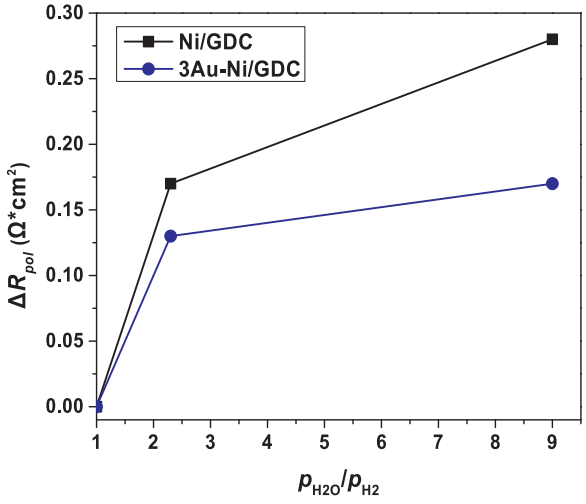

Fig. 8. R_{pol} difference (ΔR_{pol}) for the applied pH_2O/pH_2 ratios, at T = 900 °C and similar current densities (as depicted in Fig. 7) for the cell comprising (■) Ni/GDC and (●) 3 wt.% Au-Ni/GDC as cathode.

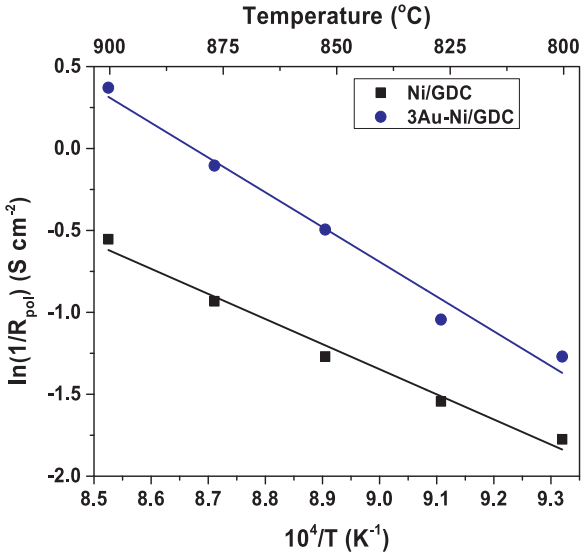

Fig. 9. Conductance (S cm^{-2}) of the (■) Ni/GDC and (●) 3 wt.% Au-Ni/GDC electrodes, derived from the R_{pol} values, in the range of 800 - 900 °C, for a reaction mixture comprising: 63 vol.% H_2O, 7 vol.% H_2 and 30 vol.% He, F_{total} = 150 cc/min (pH_2O/pH_2 = 9).

polarization losses [23,59,61].

Therefore, it is suggested that in the case of the Ni/GDC electrode there is higher degree of partial oxidation of the Ni surface at the boundaries of the electrochemical interface, resulting in higher increase of the polarization resistances and lower performance. On the other hand, the lower increment of the polarization resistances for the 3Au-Ni/GDC electrode may be primarily ascribed to the weaker interaction of water with the surface of the Au-modified electrode and the weakly adsorbed oxygen, hence resulting in a surface and an interface with a lower degree of re-oxidation.

The limited effect of water on the polarization resistance of the 3Au-Ni/GDC electrode is also in agreement with the TGA experiments, depicted in Figs. 4 and 5. Specifically, the apparent activation energy for the H_2O re-oxidation process is higher in the case of 3Au-Ni/GDC, implying weaker interaction of water and of the resulting oxidic species with the Au-modified Ni surface. This correlation would be beneficial for the kinetics of the charge transfer reaction, regarding the easier removal of the weakly-bonded O species from the Au-modified Ni surface. On the other hand, the weak interaction and consequently the

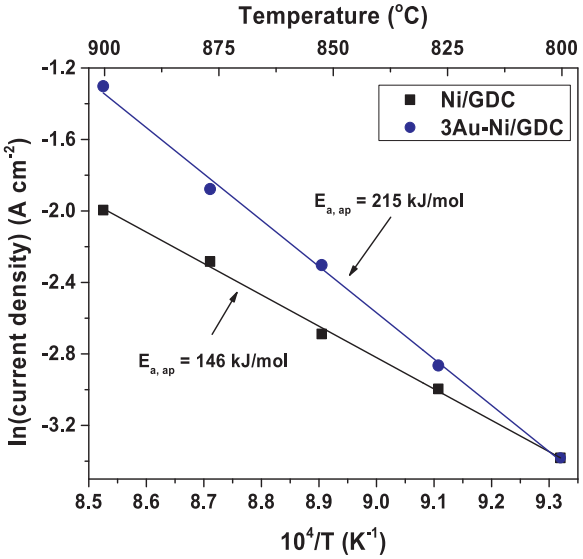

Fig. 10. Arrhenius plot of the current density (A cm^{-2}) at a constant potential value (*P = 1.1 V,* see Fig. S6 in supporting information) under H_2O electrolysis conditions. The reaction mixture comprised: 63 vol.% H_2O, 7 vol.% H_2 and 30 vol.% He, F_{total} = 150 cc/min (pH_2O/pH_2 = 9).

lower reaction rates of the water dissociation, would finally have a negative effect on the electrochemical reactions, especially at temperatures below 800 °C, due to lower oxygen coverage.

The above are explicitly reflected on the electrocatalytic rates of water electrolysis, in Figs. 6 and 10. Specifically, Fig. 10 presents the Arrhenius plots of the current densities for the two electrodes. The depicted values have been derived from the I-V curves of Fig. 6, after IR_{ohm} correction (Fig. S6 in supporting information). The latter correction was made in order to subtract any contribution from the ohmic resistances and focus on the effect of R_{pol}. Consequently, the current densities have been derived under constant Potential (i.e. 1.1 V in Fig. S6) and correspond to the depicted R_{pol} values in Fig. 7 for pH_2O/pH_2 = 9. It is shown that at 800 °C the two electrodes have essentially the same electrocatalytic rate (isokinetic point). By increasing the temperature, the rates of the cell with 3Au-Ni/GDC are enhanced and the difference between the two examined electrodes becomes significant above 850 °C. In addition, the derived apparent activation energy of the occurring electrochemical processes is once again higher for the cell with 3Au-Ni/GDC (215 kJ/mol), compared to Ni/GDC (146 kJ/mol), corroborating the remarks of Fig. 5C. Overall, the observed trend in the electrochemical performance is clearly ascribed to activated processes and it particularly suggests that the charge transfer and the electrode (e.g. H_2O conversion) processes [20,53,66,67], for the H_2O electrolysis reaction, proceed faster on the cell with the Au-modified cathode.

By comparing the results from the TGA experiments (Fig. 5) with the electrochemical measurements (Figs. 6 and 10), one noteworthy remark is that the magnitude of the water dissociation rate appears to be very low and does not support the obtained electrocatalytic rates. Indicatively, on a 10 mg cm^{-2} Ni/GDC (the amount used for electrode preparation) the disassociation rate of water (as measured in Fig. 5) is ca. 6×10^{-3} μmol s^{-1} cm^{-2} of oxygen atoms. This value is 2 orders of magnitude lower than the presented (Fig. 6A and B) electrocatalytic rates for water splitting in SOEC operation. Moreover, it has been shown in Fig. 4 that the presence of H_2 inhibits completely the thermochemical dissociation of H_2O and the subsequent oxidation of Ni/GDC. According to these observations, it is suggested that the thermochemical splitting of water, through its reaction with the surface Ni atoms, cannot be a reaction step for the electrochemical water splitting on Ni based cathodes in solid oxide electrolysis cells. This conclusion is in accordance with the theoretical work of Gu and Nikolla [50], who proposed that a valid mechanism for water splitting on Ni based cathodes, in SOECs, involves the direct electrochemical splitting of the water molecule, which is initially adsorbed on the surface Ni atom, based on the following [Reactions (7)–(9)].

$$H_2O + Ni + Vo(YSZ) + e^- \rightarrow OH^- + H_{ads} \quad (7)$$

$$OH^- + e^- \rightarrow O^{2-} + H_{ads} + Vo(YSZ) \quad (8)$$

$$2H_{ads} \rightarrow H_2 \quad (9)$$

In particular, Gu and Nikolla [50] studied several binary alloys of Ni with various metals. In this way they were able to affect the binding energy of water and oxygen on Ni, as well as the activation energy of water dissociation. Based on DFT calculations they [50] concluded that even though the increased binding energy of the water molecule on the Ni surface promotes its dissociation, however, the electrocatalytic rate is maximized at intermediate activation energies for the water dissociation and consequently at intermediate binding energies of water and O_{ads} on the modified Ni surfaces. Moreover, at low activation energies the corresponding high binding energy of the oxidic species promotes the poisoning/re-oxidation effect of the Ni surface. In the opposite case, the dissociation rate of water is the limiting factor either due to the high activation energy or due the low coverage of the water molecules, which are being induced by the low binding energy on the Ni surface. Therefore, in the present case of the 3Au-Ni/GDC electrode and at temperatures above the isokinetic point (> 800 °C), the higher activation energy is not any longer a limiting factor, whereas the lower binding energy of the O_{ads} species is less poisonous for the reactivity of the Ni surface.

4. Conclusions

Commercial NiO/GDC powder and 3 wt.% Au-NiO/GDC, prepared with the D.P. method, were compared physicochemically and electrochemically for their performance as electrode materials under H_2O electrolysis conditions.

In respect to their physicochemical properties, the samples in their oxidized (as prepared) form have similar SSA, depending on the sintering temperature. However, it was observed that after reduction the existence of Au on the modified powder enhances, to a certain extent, the coalescence of the Ni particles and possibly increases the macroporosity of the modified electrode. The surface chemical state of the samples, in the form of half cells, was investigated with in-situ XPS (H_2 reduction) measurements. In the cases of the "pristine" and re-oxidized sample, nickel is assigned to the Ni^{2+} chemical state, while in the reduced state of the samples it is mainly in its metallic form. On the other hand, GDC was found to be more reduced in the Au-modified sample. The most interesting remark from the XPS measurements is the high dispersion of Au on the Ni surface, upon reduction of the sample, which can be realized through the formation of substitutional, surface, Ni-Au solid solution.

Isothermal-TGA measurements, under H_2O/Ar conditions, indicated that the dissociative adsorption of H_2O and the oxidation rate of the surface Ni atoms, proceed with a lower rate on the 3Au-Ni/GDC sample, compared to Ni/GDC. Thus, it can be suggested that the formation of Ni-Au solid solution induces weaker bond of H_2O with the modified Ni atoms on the surface of the electrode and consequently leads to weakly adsorbed oxygen species.

The conclusions from the physicochemical characterization are in further agreement with SOEC measurements for the H_2O electrolysis reaction on ESCs. Specifically, the Au-modified electrode performed better, especially at T = 850 °C and above. The improved performance was observed in various pH_2O/pH_2 ratios, where simultaneous EIS analysis showed significantly lower R_{pol} and thus higher conductance, compared to the cell with the Ni/GDC electrode. Furthermore, by

increasing the pH_2O/pH_2 ratio the polarization resistance of the cell comprising 3Au-Ni/GDC was less affected. This improvement can be attributed to the weaker interaction of H_2O_{ads} and of the O_{ads} species, which result in a surface and an interface with lower degree of oxidation and increased (t.p.b.) length. Overall, in the case of the 3Au-Ni/GDC cathode and at temperatures higher than 800 °C, the charge transfer and electrode processes are enhanced towards a more efficient H_2O electrolysis reaction.

Acknowledgments

The authors would like to thank Dr. Stylianos G. Neophytides, Research Director at the Institute of Chemical Engineering Sciences (FORTH/ICE-HT) for the constructive comments and Ms. Katerina Govatsi, MSc. researcher at FORTH/ICE-HT, for the SEM images. The research leading to these results has received funding from the Fuel Cells and Hydrogen 2 Joint Undertaking under the project SElySOs with Grant Agreement No: 671481. This Joint Undertaking receives support from the European Union's Horizon 2020 Research and Innovation Programme and Greece, Germany, Czech Republic, France, and Norway.

Appendix A. Supplementary data

Supplementary material related to this article can be found, in the online version, at doi:https://doi.org/10.1016/j.apcatb.2018.05.017.

References

[1] S.R. Pereira, T. Fontes, M.C. Coelho, Can hydrogen or natural gas be alternatives for aviation? – A life cycle assessment, International Journal of Hydrogen Energy 39 (2014) 13266–13275.
[2] M.A. Laguna-Bercero, Recent advances in high temperature electrolysis using solid oxide fuel cells: A review, Journal of Power Sources 203 (2012) 4–16.
[3] S.D. Ebbesen, S.H. Jensen, A. Hauch, M.B. Mogensen, High Temperature Electrolysis in Alkaline Cells, Solid Proton Conducting Cells, and Solid Oxide Cells, Chemical Reviews 114 (2014) 10697–10734.
[4] Y. Tao, S.D. Ebbesen, M.B. Mogensen, Carbon Deposition in Solid Oxide Cells during Co-Electrolysis of H2O and CO2, Journal of the Electrochemical Society 161 (2014) F337–F343.
[5] A. Nechache, A. Mansuy, M. Petitjean, J. Mougin, F. Mauvy, B.A. Boukamp, M. Cassir, A. Ringuedé, Diagnosis of a cathode-supported solid oxide electrolysis cell by electrochemical impedance spectroscopy, Electrochimica Acta 210 (2016) 596–605.
[6] A. Brisse, J. Schefold, M. Zahid, High temperature water electrolysis in solid oxide cells, International Journal of Hydrogen Energy 33 (2008) 5375–5382.
[7] C. Stoots, J. O'Brien, J. Hartvigsen, Results of recent high temperature coelectrolysis studies at the Idaho National Laboratory, International Journal of Hydrogen Energy 34 (2009) 4208–4215.
[8] F. Petipas, A. Brisse, C. Bouallou, Benefits of external heat sources for high temperature electrolyser systems, International Journal of Hydrogen Energy 39 (2014) 5505–5513.
[9] C.E. Frey, Q. Fang, D. Sebold, L. Blum, N.H. Menzler, A Detailed Post Mortem Analysis of Solid Oxide Electrolyzer Cells after Long-Term Stack Operation, Journal of The Electrochemical Society 165 (2018) F357–F364.
[10] P. Moçoteguy, A. Brisse, A review and comprehensive analysis of degradation mechanisms of solid oxide electrolysis cells, International Journal of Hydrogen Energy 38 (2013) 15887–15902.
[11] Y. Zheng, J. Wang, B. Yu, W. Zhang, J. Chen, J. Qiao, J. Zhang, A review of high temperature co-electrolysis of H2O and CO2 to produce sustainable fuels using solid oxide electrolysis cells (SOECs): advanced materials and technology, Chemical Society Reviews 46 (2017) 1427–1463.
[12] A. Hauch, S.D. Ebbesen, S.H. Jensen, M. Mogensen, Solid Oxide Electrolysis Cells: Microstructure and Degradation of the Ni/Yttria-Stabilized Zirconia Electrode, Journal of the Electrochemical Society 155 (2008) B1184–B1193.
[13] E. Lay-Grindler, J. Laurencin, J. Villanova, P. Cloetens, P. Bleuet, A. Mansuy, J. Mougin, G. Delette, Degradation study by 3D reconstruction of a nickel–yttria stabilized zirconia cathode after high temperature steam electrolysis operation, Journal of Power Sources 269 (2014) 927–936.
[14] C. Graves, S.D. Ebbesen, S.H. Jensen, S.B. Simonsen, M.B. Mogensen, Eliminating degradation in solid oxide electrochemical cells by reversible operation, Nat Mater 14 (2015) 239–244.
[15] M. Chen, Y.-L. Liu, J.J. Bentzen, W. Zhang, X. Sun, A. Hauch, Y. Tao, J.R. Bowen, P.V. Hendriksen, Microstructural Degradation of Ni/YSZ Electrodes in Solid Oxide Electrolysis Cells under High Current, Journal of the Electrochemical Society 160 (2013) F883–F891.
[16] J.R. Mawdsley, J. David Carter, A. Jeremy Kropf, B. Yildiz, V.A. Maroni, Post-test evaluation of oxygen electrodes from solid oxide electrolysis stacks, International Journal of Hydrogen Energy 34 (2009) 4198–4207.
[17] A.V. Virkar, Mechanism of oxygen electrode delamination in solid oxide electrolyzer cells, International Journal of Hydrogen Energy 35 (2010) 9527–9543.
[18] J. Mougin, A. Mansuy, A. Chatroux, G. Gousseau, M. Petitjean, M. Reytier, F. Mauvy, Enhanced Performance and Durability of a High Temperature Steam Electrolysis Stack, Fuel Cells 13 (2013) 623–630.
[19] S.-D. Kim, D.-W. Seo, A.K. Dorai, S.-K. Woo, The effect of gas compositions on the performance and durability of solid oxide electrolysis cells, International Journal of Hydrogen Energy 38 (2013) 6569–6576.
[20] J. Schefold, A. Brisse, H. Poepke, 23,000 h steam electrolysis with an electrolyte supported solid oxide cell, International Journal of Hydrogen Energy 42 (2017) 13415–13426.
[21] C. Sun, U. Stimming, Recent anode advances in solid oxide fuel cells, Journal of Power Sources 171 (2007) 247–260.
[22] M. Chen, J.V.T. Høgh, J.U. Nielsen, J.J. Bentzen, S.D. Ebbesen, P.V. Hendriksen, High Temperature Co-Electrolysis of Steam and CO2 in an SOC Stack: Performance and Durability, Fuel Cells 13 (2013) 638–645.
[23] F. Tietz, D. Sebold, A. Brisse, J. Schefold, Degradation phenomena in a solid oxide electrolysis cell after 9000 h of operation, Journal of Power Sources 223 (2013) 129–135.
[24] Q. Fu, J. Schefold, A. Brisse, J.U. Nielsen, Durability Testing of a High-Temperature Steam Electrolyzer Stack at 700 °C, Fuel Cells 14 (2014) 395–402.
[25] V. Singh, H. Muroyama, T. Matsui, S. Hashigami, T. Inagaki, K. Eguchi, Feasibility of alternative electrode materials for high temperature CO2 reduction on solid oxide electrolysis cell, Journal of Power Sources 293 (2015) 642–648.
[26] S.-W. Kim, M. Park, H. Kim, K.J. Yoon, J.-W. Son, J.-H. Lee, B.-K. Kim, J.-H. Lee, J. Hong, Catalytic Effect of Pd-Ni Bimetallic Catalysts on High-Temperature Co-Electrolysis of Steam/CO2 Mixtures, Journal of The Electrochemical Society 163 (2016) F3171–F3178.
[27] P. Kim-Lohsoontorn, Y.-M. Kim, N. Laosiripojana, J. Bae, Gadolinium doped ceria-impregnated nickel-yttria stabilised zirconia cathode for solid oxide electrolysis cell, International Journal of Hydrogen Energy 36 (2011) 9420–9427.
[28] R. Nishida, P. Puengjinda, H. Nishino, K. Kakinuma, M.E. Brito, M. Watanabe, H. Uchida, High-performance electrodes for reversible solid oxide fuel cell/solid oxide electrolysis cell: Ni-Co dispersed ceria hydrogen electrodes, RSC Advances 4 (2014) 16260–16266.
[29] P. Kim-Lohsoontorn, J. Bae, Electrochemical performance of solid oxide electrolysis cell electrodes under high-temperature coelectrolysis of steam and carbon dioxide, Journal of Power Sources 196 (2011) 7161–7168.
[30] D.K. Niakolas, M. Athanasiou, V. Dracopoulos, I. Tsiaoussis, S. Bebelis, S.G. Neophytides, Study of the synergistic interaction between nickel, gold and molybdenum in novel modified NiO/GDC cermets, possible anode materials for CH4 fueled SOFCs, Applied Catalysis A: General 456 (2013) 223–232.
[31] C. Neofytidis, M. Athanasiou, S.G. Neophytides, D.K. Niakolas, Sulfur Tolerance of Au–Mo–Ni/GDC SOFC Anodes Under Various CH4 Internal Steam Reforming Conditions, Topics in Catalysis 58 (2015) 1276–1289.
[32] D.K. Niakolas, Sulfur poisoning of Ni-based anodes for Solid Oxide Fuel Cells in H/C-based fuels, Applied Catalysis A: General 486 (2014) 123–142.
[33] C. Neofytidis, V. Dracopoulos, S.G. Neophytides, D.K. Niakolas, Electrocatalytic performance and carbon tolerance of ternary Au-Mo-Ni/GDC SOFC anodes under CH4-rich Internal Steam Reforming conditions, Catalysis Today (2017).
[34] D.K. Niakolas, J.P. Ouweltjes, G. Rietveld, V. Dracopoulos, S.G. Neophytides, Au-doped Ni/GDC as a new anode for SOFCs operating under rich CH4 internal steam reforming, International Journal of Hydrogen Energy 35 (2010) 7898–7904.
[35] S. Souentie, M. Athanasiou, D.K. Niakolas, A. Katsaounis, S.G. Neophytides, C.G. Vayenas, Mathematical modeling of Ni/GDC and Au–Ni/GDC SOFC anodes performance under internal methane steam reforming conditions, Journal of Catalysis 306 (2013) 116–128.
[36] D.K. Niakolas, C.S. Neofytidis, S.G. Neophytides, Effect of Au and/or Mo Doping on the Development of Carbon and Sulfur Tolerant Anodes for SOFCs—A Short Review, Frontiers in Environmental Science (2017) 5.
[37] X. Yu, G. Li, XPS study of cerium conversion coating on the anodized 2024 aluminum alloy, Journal of Alloys and Compounds 364 (2004) 193–198.
[38] E. Kordouli, L. Sygellou, C. Kordulis, K. Bourikas, A. Lycourghiotis, Probing the synergistic ratio of the NiMo/γ-Al2O3 reduced catalysts for the transformation of natural triglycerides into green diesel, Applied Catalysis B: Environmental 209 (2017) 12–22.
[39] X. Du, D. Zhang, L. Shi, R. Gao, J. Zhang, Morphology Dependence of Catalytic Properties of Ni/CeO2 Nanostructures for Carbon Dioxide Reforming of Methane, The Journal of Physical Chemistry C 116 (2012) 10009–10016.
[40] W. Shan, M. Luo, P. Ying, W. Shen, C. Li, Reduction property and catalytic activity of Ce1 − XNiXO2 mixed oxide catalysts for CH4 oxidation, Applied Catalysis A: General 246 (2003) 1–9.
[41] M. Bienzle, T. Oishi, F. Sommer, Thermodynamics and local atomic arrangements of gold-nickel alloys, Journal of Alloys and Compounds 220 (1995) 182–188.
[42] L. Pleth Nielsen, F. Besenbacher, I. Stensgaard, E. Laegsgaard, C. Engdahl, P. Stoltze, K.W. Jacobsen, J.K. Nørskov, Initial growth of Au on Ni(110): Surface alloying of immiscible metals, Physical Review Letters 71 (1993) 754–757.
[43] F. Besenbacher, I. Chorkendorff, B.S. Clausen, B. Hammer, A.M. Molenbroek, J.K. Norskov, I. Stensgaard, Design of a surface alloy catalyst for steam reforming, Science 279 (1998) 1913–1915.
[44] D. Sarantaridis, A. Atkinson, Redox Cycling of Ni-Based Solid Oxide Fuel Cell Anodes: A Review, Fuel Cells 7 (2007) 246–258.
[45] M. Ettler, H. Timmermann, J. Malzbender, A. Weber, N.H. Menzler, Durability of Ni anodes during reoxidation cycles, Journal of Power Sources 195 (2010) 5452–5467.

[46] A. Atkinson, D.W. Smart, Transport of Nickel and Oxygen during the Oxidation of Nickel and Dilute Nickel/Chromium Alloy, Journal of The Electrochemical Society 135 (1988) 2886–2893.
[47] L.P. Matte, A.S. Kilian, L. Luza, M.C.M. Alves, J. Morais, D.L. Baptista, J. Dupont, F. Bernardi, Influence of the CeO2 Support on the Reduction Properties of Cu/CeO2 and Ni/CeO2 Nanoparticles, The Journal of Physical Chemistry C 119 (2015) 26459–26470.
[48] S. Ghosh, S. Hariharan, A.K. Tiwari, Water Adsorption and Dissociation on Copper/Nickel Bimetallic Surface Alloys: Effect of Surface Temperature on Reactivity, The Journal of Physical Chemistry C 121 (2017) 16351–16365.
[49] L.-Y. Gan, R.-Y. Tian, X.-B. Yang, H.-D. Lu, Y.-J. Zhao, Catalytic Reactivity of CuNi Alloys toward H2O and CO Dissociation for an Efficient Water–Gas Shift: A DFT Study, The Journal of Physical Chemistry C 116 (2012) 745–752.
[50] X.-K. Gu, E. Nikolla, Fundamental Insights into High-Temperature Water Electrolysis Using Ni-Based Electrocatalysts, The Journal of Physical Chemistry C 119 (2015) 26980–26988.
[51] P. Kratzer, B. Hammer, J.K. No/rskov, A theoretical study of CH4 dissociation on pure and gold-alloyed Ni(111) surfaces, The Journal of Chemical Physics 105 (1996) 5595–5604.
[52] B. Hammer, J.K. Nørskov, Theoretical surface science and catalysis—calculations and concepts, Advances in Catalysis, Academic Press, 2000, pp. 71–129.
[53] J. Schefold, A. Brisse, H. Poepke, Long-term Steam Electrolysis with Electrolyte-Supported Solid Oxide Cells, Electrochimica Acta 179 (2015) 161–168.
[54] S. Primdahl, M. Mogensen, Gas Conversion Impedance: A Test Geometry Effect in Characterization of Solid Oxide Fuel Cell Anodes, Journal of The Electrochemical Society 145 (1998) 2431–2438.
[55] O.H. Kwon, G.M. Choi, Electrical conductivity of thick film YSZ, Solid State Ionics 177 (2006) 3057–3062.
[56] B.E. McNealy, J. Jiang, J.L. Hertz, A. Precise, Reduced-Parameter Model of Thin Film Electrolyte Impedance, Journal of The Electrochemical Society 162 (2015) F537–F546.
[57] D. Kek, P. Panjan, E. Wanzenberg, J. Jamnik, Electrical and microstructural investigations of cermet anode/YSZ thin film systems, Journal of the European Ceramic Society 21 (2001) 1861–1865.
[58] Ö. Çelikbilek, E. Siebert, D. Jauffrès, C.L. Martin, E. Djurado, Influence of sintering temperature on morphology and electrochemical performance of LSCF/GDC composite films as efficient cathode for SOFC, Electrochimica Acta 246 (2017) 1248–1258.
[59] D. The, S. Grieshammer, M. Schroeder, M. Martin, M. Al Daroukh, F. Tietz, J. Schefold, A. Brisse, Microstructural comparison of solid oxide electrolyser cells operated for 6100 h and 9000 h, Journal of Power Sources 275 (2015) 901–911.
[60] L. Li, F. Jin, Y. Shen, T. He, Cobalt-free double perovskite cathode GdBaFeNiO5 + δ and electrochemical performance improvement by Ce0.8Sm0.2O1.9 impregnation for intermediate-temperature solid oxide fuel cells, Electrochimica Acta 182 (2015) 682–692.
[61] V. Papaefthimiou, D.K. Niakolas, F. Paloukis, D. Teschner, A. Knop-Gericke, M. Haevecker, S. Zafeiratos, Operando observation of nickel/ceria electrode surfaces during intermediate temperature steam electrolysis, Journal of Catalysis 352 (2017) 305–313.
[62] H. Yokokawa, H. Tu, B. Iwanschitz, A. Mai, Fundamental mechanisms limiting solid oxide fuel cell durability, Journal of Power Sources 182 (2008) 400–412.
[63] A. Faes, A. Hessler-Wyser, A. Zryd, J. Van herle, A Review of RedOx Cycling of Solid Oxide Fuel Cells Anode, Membranes 2 (2012) 585.
[64] T. Matsui, R. Kishida, J.-Y. Kim, H. Muroyama, K. Eguchi, Performance Deterioration of Ni–YSZ Anode Induced by Electrochemically Generated Steam in Solid Oxide Fuel Cells, Journal of The Electrochemical Society 157 (2010) B776–B781.
[65] T. Matsui, H. Fujii, A. Ozaki, T. Takeuchi, R. Kikuchi, K. Eguchi, Degradation Behavior of Ni – ScSZ Cermet Anode under Various Humidified Conditions for Solid Oxide Fuel Cells, Journal of The Electrochemical Society 154 (2007) B1237–B1241.
[66] A. Nechache, M. Cassir, A. Ringuedé, Solid oxide electrolysis cell analysis by means of electrochemical impedance spectroscopy: A review, Journal of Power Sources 258 (2014) 164–181.
[67] E.-C. Shin, P.-A. Ahn, H.-H. Seo, J.-M. Jo, S.-D. Kim, S.-K. Woo, J.H. Yu, J. Mizusaki, J.-S. Lee, Polarization mechanism of high temperature electrolysis in a Ni–YSZ/YSZ/LSM solid oxide cell by parametric impedance analysis, Solid State Ionics 232 (2013) 80–96.